

XXII. NEUROLOGY*

L. Stark
F. H. Baker
R. W. Cornew
H. T. Hermann
J. C. Houk, Jr.
G. Masek
E. G. Merrill
R. Millecchia

T. A. Rowe
E. Sadler
A. A. Sandberg
Susanne Shuman
J. I. Simpson
Gabriella W. Smith
I. Sobel

S. F. Stanten
A. Troelstra
E. C. Van Horn, Jr.
G. L. Wickelgren
P. A. Willis
S. Yasui
L. R. Young
B. L. Zuber

A. EYE CONVERGENCE

1. Improved Measuring Device

A pair of photocells (Clairex, CL-602), sensitive in the red region, have been mounted on eyeglass frames and connected into a bridge circuit. The subject's face is illuminated from above and at a distance of approximately 8 inches with a red light. These glasses offer several advantages over those previously used^{1,2}; they are simple to construct; they are linear over a range of ± 10 degrees; and, primarily, they reduce fatigue and strain caused by the rather intense visible light used with earlier glasses. The time constant of the improved glasses has been determined experimentally to be approximately 30 msec.

2. Results of Experiments

a. Step Response

Sample step responses appear in Fig. XXII-1. These are characterized by an

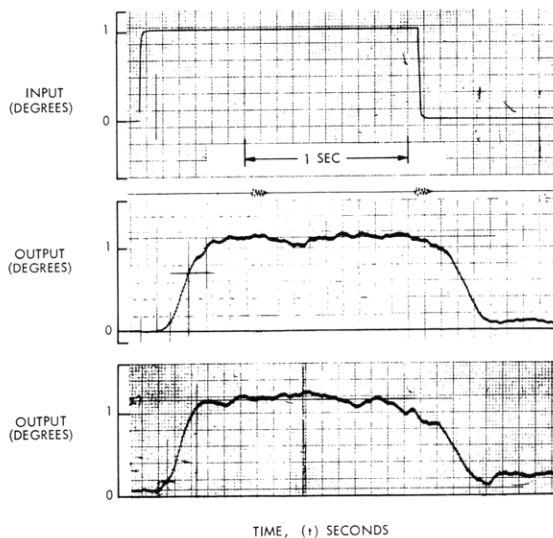


Fig. XXII-1. Step response.

*This research is supported in part by the U. S. Public Health Service (B-3055-3, B-3090-3, 38101-22), the Office of Naval Research (Nonr-1841 (70)), the Air Force (AF33(616)-7588, AFAOSR 155-63), and the Army Chemical Corps (DA-18-108-405-Cml-942); and in part by the National Institutes of Health (Grant MH-04734-03).

(XXII. NEUROLOGY)

average delay time of approximately 128 msec and an average rise time (between 90 per cent and 10 per cent amplitude) of 200 msec. The results were roughly the same, whether steps were predictable or unpredictable.

b. Frequency Response

Bode plots resulting from predictable and unpredictable inputs are shown in Fig. XXII-2. These experiments were carried out by using a dc level corresponding to an apparent distance of 33.5 cm (angle of convergence, 5.1 degrees) and an amplitude corresponding to a change in apparent distance of approximately 5 cm (change of angle of convergence, 0.85 degrees). At this dc level, the apparent distance of the image is equal to the real distance. The dc level and amplitude were selected after

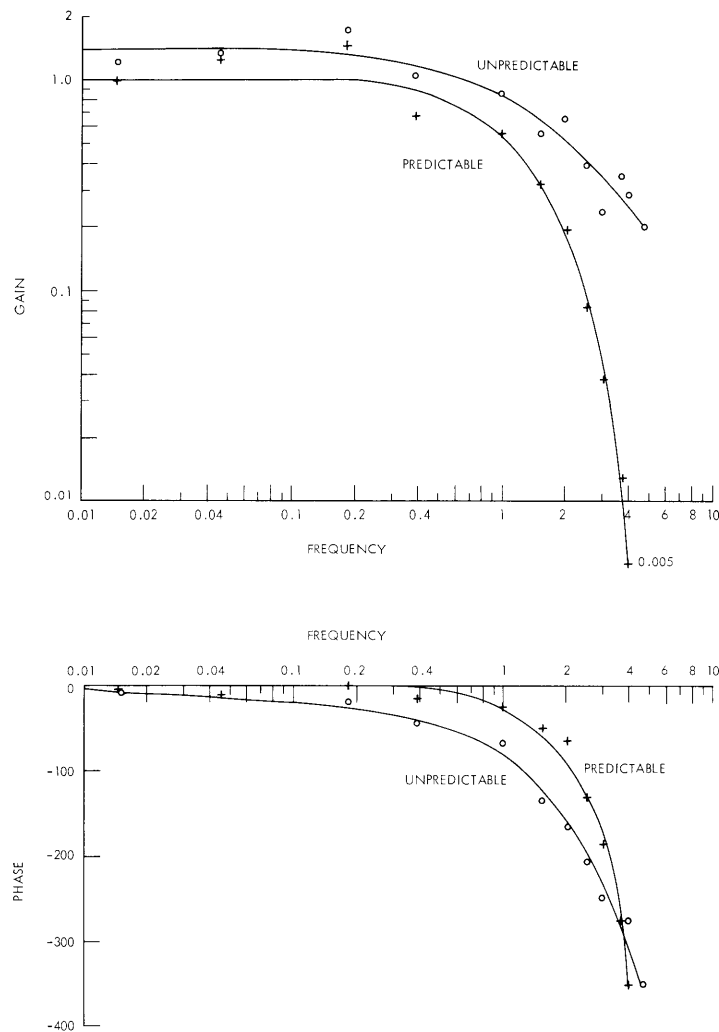


Fig. XXII-2. Bode plots.

it was found that using larger amplitudes, approximately 2.5 degrees, and dc levels differing from the real distance of the image resulted in the introduction of serious errors into the recorded data. When large amplitudes are used the subject is unable to keep the image in sharp focus over the entire range. In the part of the range in which the image appears out of focus, fusion is lost. The problem is further complicated if the subject attempts to adjust his accommodation for an image that might appear to be at a distance quite different from the real distance between the subject's eyes and the image. For these reasons a small amplitude about a dc level at which real and apparent distances are equal was selected to optimize accommodation.

The G. E. 225 computer was used to produce stimuli and to analyze responses. For frequencies less than 1 cps, results for the Bode plots were obtained in separate predictable and unpredictable input experiments. These gave characteristic gain and phase values for low frequencies. For frequencies greater than 1 cps, single frequencies and mixed-frequency groups were presented during the same experiment. In the latter case the order of presentation of single frequencies, groups, and frequencies within any given group was randomized.³

It is clear from the phase curves that a predictor apparatus operates to increase the phase margin near the -180 -degree crossover frequency of the unpredictable curve.

c. High-Gain Oscillations

The unpredictable phase curve shows that the system has a phase lag of 180 degrees at a frequency of approximately 2.3 cps. If the loop gain of the system were sufficiently

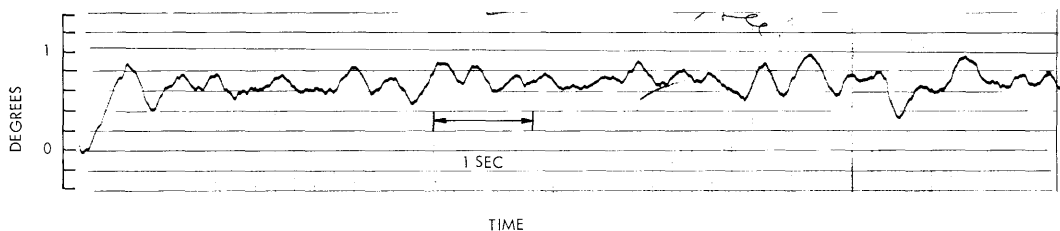


Fig. XXII-3. High-Gain oscillations.

high, one would expect the system to oscillate at this frequency. When an artificial loop was placed around the system and the gain increased, the system was found to oscillate spontaneously at an average frequency of 2.5 cps. Sample records are shown in Fig. XXII-3.

B. L. Zuber, A. Troelstra, L. Stark

(XXII. NEUROLOGY)

References

1. L. Stark and A. Sandberg, A simple instrument for measuring eye movement, Quarterly Progress Report No. 62, Research Laboratory of Electronics, M.I.T., July 15, 1961, pp. 268-270.
2. G. P. Nelson, L. Stark, and L. R. Young, Phototube glasses for measuring eye movements, Quarterly Progress Report No. 67, Research Laboratory of Electronics, M.I.T., October 15, 1962, pp. 214-215.
3. B. L. Zuber and L. Stark, Eye convergence, Quarterly Progress Report No. 68, Research Laboratory of Electronics, M.I.T., January 15, 1963, pp. 232-234.

B. ASSOCIATED EYE MOVEMENTS

The subject is presented with a target, as shown in Fig. XXII-4, by means of an X-Y recorder. The target movement, sinusoidal (0.3 cps) or stepwise (0.1 cps), is seen only with the right eye; the left eye is occluded by an opaque screen. The

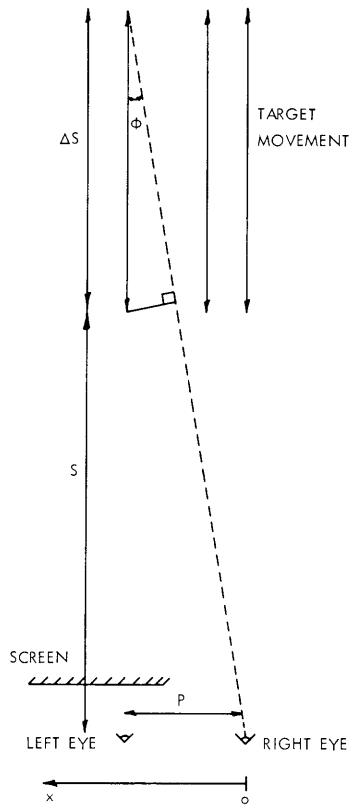


Fig. XXII-4. Experimental arrangement.

subject is asked to fixate the target and to keep it in focus. Movements of the left eye, which has no visual input, are measured. Visual input to the right eye may be resolved into a depth perception and a target displacement. Depth perception is a function of $\cos \phi$:

$$\text{Depth perception} = \Delta S \cos \phi = \frac{\Delta S(S+\Delta S)}{\sqrt{(S+\Delta S)^2 + X^2}} \approx \Delta S,$$

since $(S+\Delta S)^2 \gg X^2$ for the experimental conditions ($S = 21$ cm, $\Delta S = 15$ cm, $X_{\max} = 6$ cm). Consequently, the depth perception is more or less independent of the value of X .

Target displacement is a function of $\sin \phi$:

$$\text{Target displacement} = \Delta S \sin \phi = \frac{(\Delta S)X}{\sqrt{(S+\Delta S)^2 + X^2}} \approx \frac{(\Delta S)X}{S + \Delta S}.$$

Two types of associated movements of the left eye can result from the input to the right eye: accommodative convergence (AC) and associated tracking (AT).

1. Accommodative Convergence Movements

Accommodative convergence (or divergence) movements are defined as those movements resulting when the right eye changes its accommodation. For example, if the target is moved in the optical axis of the right eye, the left eye will follow roughly the target movement, even though the left eye receives no visual information and there are no movements of the right eye. With reference to Fig. XXII-4 and by assuming some gain for accommodative convergence, movement of the left eye which results from accommodative convergence will be

$$AC = G_{AC} \frac{(\Delta S)P}{(S+\Delta S)\sqrt{S^2 + X^2}} \frac{360}{2\pi} \text{ degrees.} \quad (1)$$

Gain will be frequency dependent, but in this experiment, in which low frequencies are used, that frequency dependence will be neglected. Furthermore, it will be assumed that G_{AC} depends only on the depth perception of the right eye and is independent of ϕ , and that G_{AC} is independent of additional visual information (for example, target displacement).

G_{AC} can be determined experimentally by measuring the movement of the covered and uncovered left eye when the target is moved in the optical axis of the right eye.

2. Associated Tracking Movements

Associated tracking movements of the left eye result when the right eye moves while tracking the target. These movements are opposite in sign compared with accommodative convergence movements. They are assumed to be proportional to the target displacement seen by the right eye.

$$AT = -G_{AT} \frac{(\Delta S)X}{(S+\Delta S) \sqrt{S^2 + X^2}} \frac{360}{2\pi} \text{ degrees.} \quad (2)$$

The definition of G_{AT} is similar to that for G_{AC} , except that G_{AT} is assumed to depend only on target displacement. G_{AT} is measured experimentally by presenting only a target displacement to the right eye and measuring the movement of the left eye, covered and uncovered. For three values of ϕ approximately 10 degrees apart the values of G_{AT} obtained are 1.25, 1.15, and 1.15.

3. Combined Associated Movements

In general, the right eye will receive information that consists of both depth perception and target displacement. If these two kinds of information contribute independently

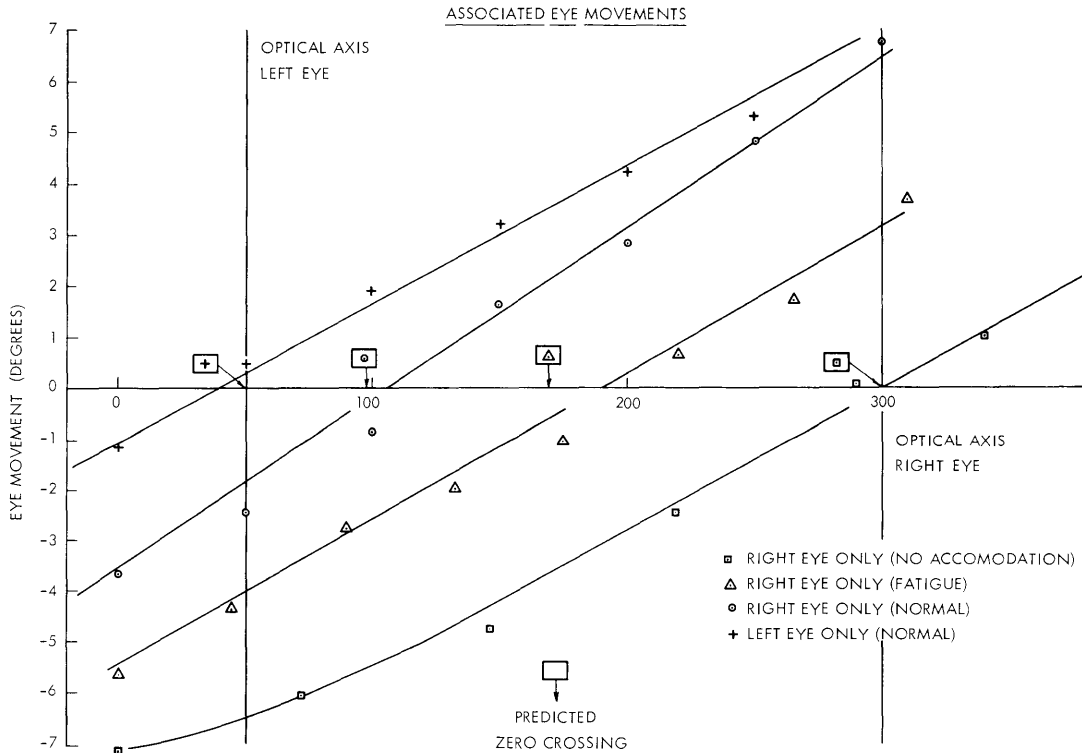


Fig. XXII-5. Associated movements of the left eye.

to the associated movement of the left eye, Eqs. 1 and 2 may be combined. In this experiment, then, the net movement of the left eye may be represented by

$$AC + AT = \frac{\Delta S}{(S+\Delta S) \sqrt{S^2 + X^2}} \frac{360}{2\pi} (PG_{AC} - XG_{AT}) \text{ degrees} \quad (3)$$

or

$$AC + AT = \frac{24}{\sqrt{440 + X^2}} (6G_{AC} - XG_{AT}) \text{ degrees.} \quad (4)$$

From Eq. 4 it is clear that the value of X for which there will be no associated movement of the left eye is given by

$$6G_{AC} - XG_{AT} = 0. \quad (5)$$

The value of $X_{\text{zero crossing}}$ as predicted by Eq. 5 was compared with the experimentally measured value for three different conditions of the eyes. The results are shown in Table XXII-1 and Fig. XXII-5.

Table XXII-1. Values of predicted $X_{\text{zero crossing}}$ for three different conditions of the eyes (left eye covered).

Condition of eyes	G_{AC}	G_{AT}	$X_{\text{zero crossing}}$ (cm)	$X_{\text{zero crossing}}$ (arbitrary abscissa of Fig. XXII-5)
Normal	0.95	1.17	4.9	97
Highly Fatigued	0.62	1.20	3.1	170
Not Accommodating	0	—	0	300

The experimental results clearly indicate that G_{AC} and G_{AT} are independent of each other, G_{AC} is greatly influenced by the degree of fatigue of the eyes, and G_{AT} is relatively free from fatigue.

A. Troelstra, L. Stark

C. ARTIFICIAL PHOTOSENSITIZATION OF THE CRAYFISH VENTRAL NERVE CORD

It has been known for a long time that muscle and nerve tissue after being stained with certain organic dyes becomes photosensitive. This report will consider the problem of classifying these artificial photic responses and associating these responses with physiological sites, presumably responsible for their origination.

1. Method

The artificial photoreceptor used in the experiment was the ventral nerve cord of the crayfish *Cambarus astacus*, which had been stained with Methylene blue (1:10,000)

(XXII. NEUROLOGY)

for 90 minutes. The experiment was performed in an electrically insulated humidity chamber (100 per cent saturation, 10°C) which kept the nerve cord active for many hours.

The nerve cord was stimulated with a standard microscope illuminator, the light being focused to a spot 2.55 mm in diameter (0.06 lumen/mm²).

The nerve pulses were recorded by using gross platinum hook electrodes. These pulses were fed into an electronic amplifying and windowing system and then displayed on a pen recorder.

2. Results of Experiment

Three characteristic features of the nerve responses were evident. The first was an excitatory response, an increase in the nerve pulse rate when the nerve was stimulated with light. The second was an inhibitory response, a decrease in the pulse rate when stimulated. The third was an "off" response, an increase in the pulse rate at the cessation of the stimulation.

A physiological location of the origin of each of these responses was made by carefully noting the site of stimulation associated with each response. An excitatory response occurred when the nerve cord was stimulated at a ganglion, while an inhibitory response, followed by an "off" response, occurred when a segment of axon was stimulated. Figure XXII-6 shows a recording of each of these responses and of a composite response obtained by stimulating a ganglion and a segment of axon simultaneously.

Using the electronic windowing technique, I found that only a small number of nerve fibers contributed to the photic response, namely the "B" fibers.

The minimum stimulus needed to evoke a response was found to be 0.4 second of

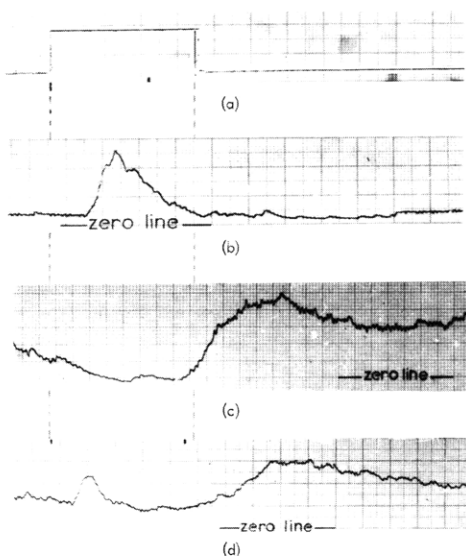


Fig. XXII-6. Response of artically photosensitized crayfish ventral nerve cord.
(a) Light stimulus (0.06 lumen/mm²);
(b) Excitatory response of ganglion;
(c) Inhibitory and "off" response of axon;
(d) Composite response.

illumination from the microscope illuminator, which, on other terms, is approximately 25 photons/dye molecule (this is assumed to be the response of a single B fiber).

3. Minimum Photon Computation

The number of photons that are incident on the nerve can be calculated by using

$$\int_{\lambda_1}^{\lambda_2} N_I h c \frac{d\lambda}{\lambda^2} = E_T,$$

where

N_I is incident number of photons;

$\lambda_1 - \lambda_2 = 400 \text{ m}\mu - 700 \text{ m}\mu$, wavelength range of visible spectrum;

$h = 6.62 \times 10^{-27}$ erg-sec, Planck's constant;

$c = 3 \times 10^{10}$ cm/sec, speed of light;

$E_T = \text{kPAT}$, total energy in ergs incident on nerve.

Here,

$P = 0.06$ lumens/mm², power of light source;

$A = 2.6 \times 10^{-2}$ mm², stimulated area of nerve fiber;

$T = 0.4$ sec, minimum stimulation time;

$k = 1.61 \times 10^4$ (ergs/sec)/lumen, conversion factor.

Thus the incident number of photons is

$$N_I = 4.5 \times 10^{10} \text{ photons.}$$

The Methylene blue dye absorbs approximately 20 per cent of the incident illumination; therefore the number of photons absorbed by the dye is

$$N_A = 0.2 N_I = 9 \times 10^{10} \text{ photons.}$$

In a Methylene blue (1:10,000) solution the number of dye molecules per cubic centimeter is approximately

$$n = 1.8 \times 10^{17} \text{ molecules/cc.}$$

At this concentration and for a staining period of 90 minutes the nerve fiber takes up approximately 10 per cent of the dye. Therefore the number of dye molecules in the stimulated segment of nerve can be calculated from $N_M = 10\% nV$, where V , the volume of the stimulated nerve fiber, is 2×10^{-7} cc. Thus $N_M = 3.6 \times 10^9$ dye molecules.

We finally can calculate the minimum number of photons per dye molecule needed to evoke a response.

$$N_o = N_A / N_M = 25 \text{ photons/dye molecule.}$$

4. Discussion

The experimental results suggest the existence of two types of artificial photoreceptors, an excitatory one and an inhibitory one, the excitatory photoreceptor being localized in the vicinity of the ganglia and the inhibitory photoreceptor being localized in the vicinity of the axons. They also suggest that the receptors are associated primarily with the B fibers that seem to have some generalized photosensitive properties.

R. Millecchia

D. HEAD MOVEMENTS

An investigation of the manner in which the rotations of the head aid human visual tracking has been initiated. The purpose of the work to date has been threefold. First, an efficient experimental procedure has been designed to minimize the time that is necessary to record data from a particular subject. Second, a variety of excitations has been applied to subjects in an attempt to characterize typical responses. Third, under the hypothesis that allowing movement of the head serves to extend the frequency response of the visual tracking system, a set of preliminary experiments with sums of sinusoids used as excitations has been performed.

A narrow slit of light (7.5×0.25 cm) is projected by means of a slit projector onto a Sanborn galvanometer-driven mirror, and is reflected onto a horizontal semicircular projection screen. The projection screen has a radius of curvature of 2.7 meters and the subject is seated at the center of screen curvature. Thus, a target angle is generated in proportion to the voltage that is denoted the target voltage. Figure XXII-7 shows the relative positions of the major apparatus.

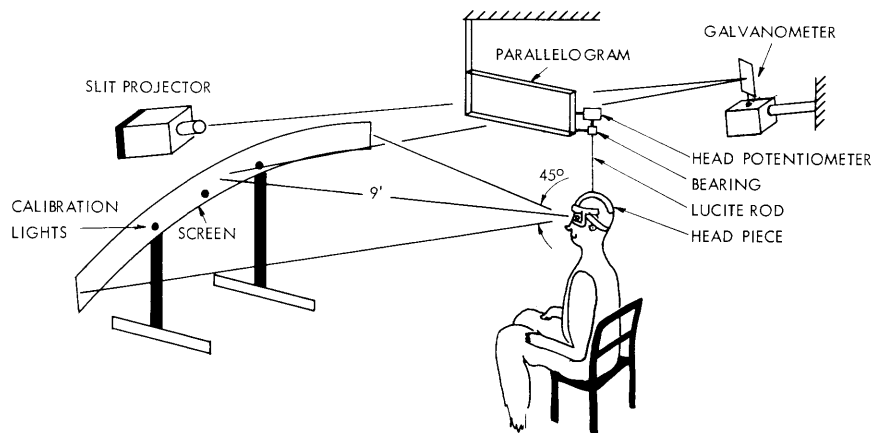


Fig. XXII-7. Relative positions of major apparatus.

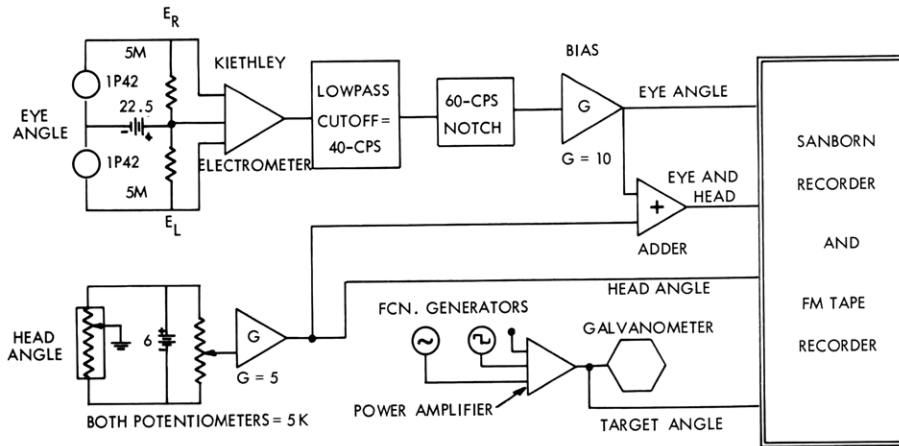


Fig. XXII-8. Simplified block diagram of eye angle and head angle instrumentation.

To measure head angle, a plastic headpiece was designed which snugly fits a variety of head sizes and shapes. The headpiece transmits information concerning head rotations in the horizontal plane to a potentiometer, which is connected in a bridge circuit. The headpiece also contains the two photocells and light bulbs used to measure lateral

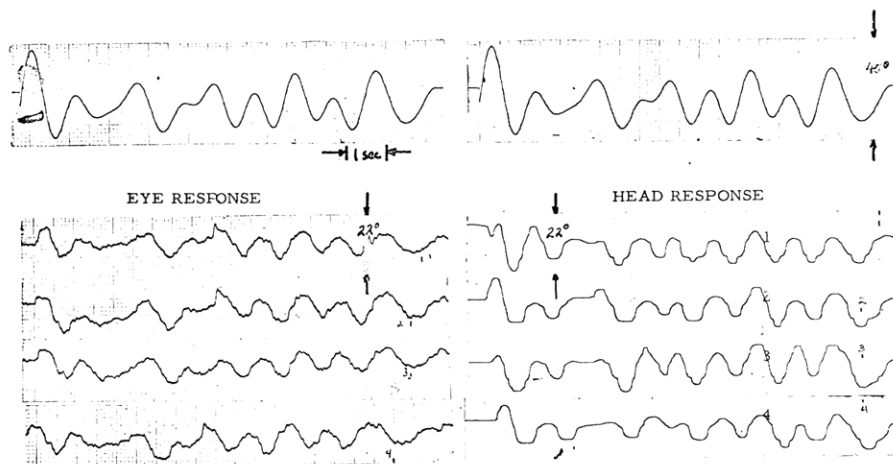


Fig. XXII-9. Four responses to sum of 5 sinusoids.

eye angle with respect to the head.¹ The method of constraining the head with the head-piece does not interfere at all mechanically, nor to a great extent psychologically, with the natural movements of the head. Figure XXII-8 shows a simplified flow diagram of the head- and eye-angle measurement instrumentation.

By prerecording the various excitations, sums of sinusoids, on FM tape and by recording the three responses (head, eye, and head-plus-eye angles) simultaneously

(XXII. NEUROLOGY)

on tape, an existing G. E. 225 computer program (MITMR) was used to analyze sequentially the head, eye, and head-plus-eye angles. Figure XXII-9 shows four head-and-eye angle responses to a sum of 5 sinusoids.

1. Single Sinusoid Responses

Several characteristics occur consistently in the single-sinusoid responses. Qualitatively, for a constant-amplitude target angle the individual gains of eye and head angle vary with time; however, the head-plus-eye angle gain remains constant with time. Zero shifts in eye angle and head angle are as large as 20 per cent of the respective amplitudes, but are complementary, so that no zero shift occurs in the head-plus-eye response. Head angle gain (or normalized amplitude) varies with target amplitude; furthermore, the Bode asymptotic intersection frequency decreases as target-angle amplitude decreases.

2. Square Step Responses

Figure XXII-10 shows a typical response to a square step of target angle. Characteristic discrete jumps in head angle occur with intervening periods ranging from

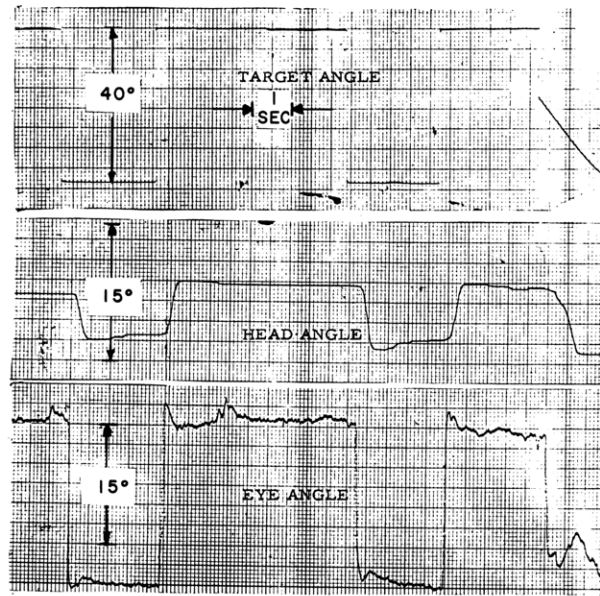


Fig. XXII-10. Typical responses to square step input.

200 msec to 600 msec and amplitudes of 0.1-0.4 degrees.² Latencies of eye response are not dependent upon whether the head is free or fixed, but range from 200 msec to 300 msec. Average response of head movement is 400 msec.

G. Masek

References

1. L. Stark and A. Sandberg, A simple instrument for measuring eye movements, Quarterly Progress Report No. 62, Research Laboratory of Electronics, M. I. T., July 15, 1961, pp. 268-270.
2. L. R. Young, A Sample Data Model for Eye Tracking Movements, Sc. D. Thesis, Department of Aeronautics and Astronautics, M. I. T., May 11, 1962.

E. MODIFICATION OF INPUT PARAMETERS FOR EKG PATTERN-RECOGNITION ANALYSIS

The G. E. 225 computer with integral analog-to-digital and digital-to-analog equipment has been incorporated into an experimental system (Fig. XXII-11) for remote on-line medical diagnostic study. This system applies pattern-recognition techniques to the classification and automatic diagnosis of clinical electrocardiograms.

A program for the IBM 7090 computer has been developed for pattern recognition which uses a system of multiple adaptive matched filters. The recognition system appears to operate in a manner that is similar to the human pattern-recognition process that is the conventional means used for EKG analysis. The filter analyses are made in the time domain that is such that no Fourier analysis is required. The over-all program involves a variety of normalization, weighting, comparison, decision, modification, and adapting operations.

A complete diagnosis of the EKG requires an analysis of all three vector components ($X(t)$, $Y(t)$, $Z(t)$) of the spatial vector signal. Recent investigations of the pattern-recognition system treat only one vector component (X , Y or Z) of the signal. Methods have been investigated to treat the vector components as related patterns and to associate pertinent information from one component to another to form one function (X, Y, Z). By a reduction of input data to a form that is more suitable for the pattern-recognition system, the computer diagnosis of the EKG can be simplified.

The function (X, Y, Z) must meet the following criteria to be useful in the pattern-recognition system:

- (a) It must be similar for each set of data corresponding to one particular diagnosis.
- (b) It must be unique for data corresponding to different diagnoses.

The G. E. 225 computer has been programmed to determine a variety of geometrical parameters of the EKG spatial curve. The functions being investigated include spherical coordinates, first derivative of arc length, and curvature. Each parameter is a function of time so as to coincide with the recognition system. Figures XXII-12 and XXII-13 show typical results from two different data sets.

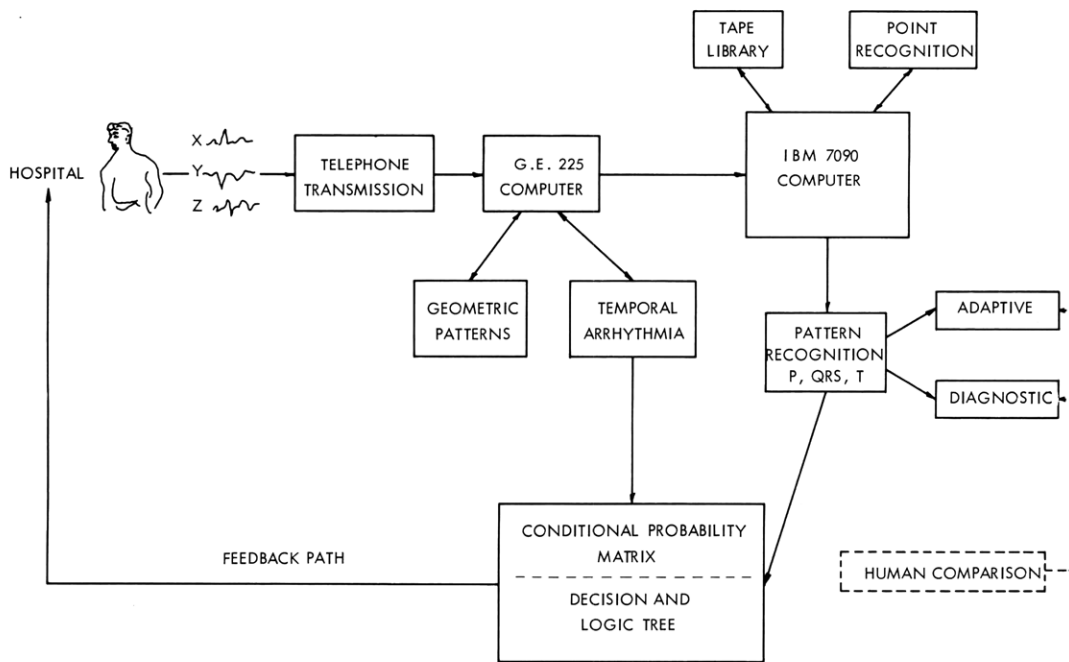


Fig. XXII-11. The G. E. 225 computer with integral analog-to-digital and digital-to-analog equipment. (Geometric patterns modify input parameters.)

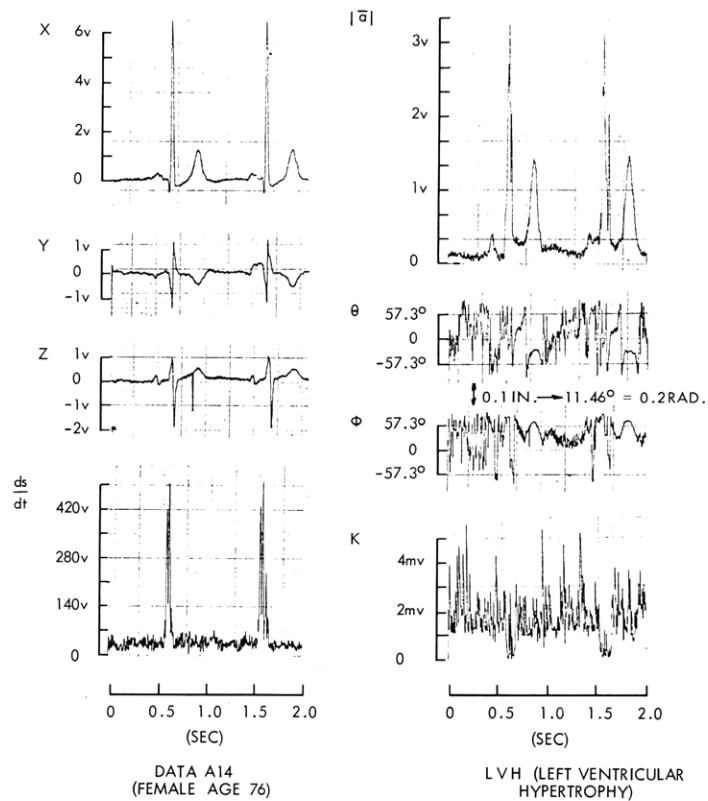


Fig. XXII-12. The EKG vector and associated functions for a female of age 76 years with left ventricular hypertrophy.

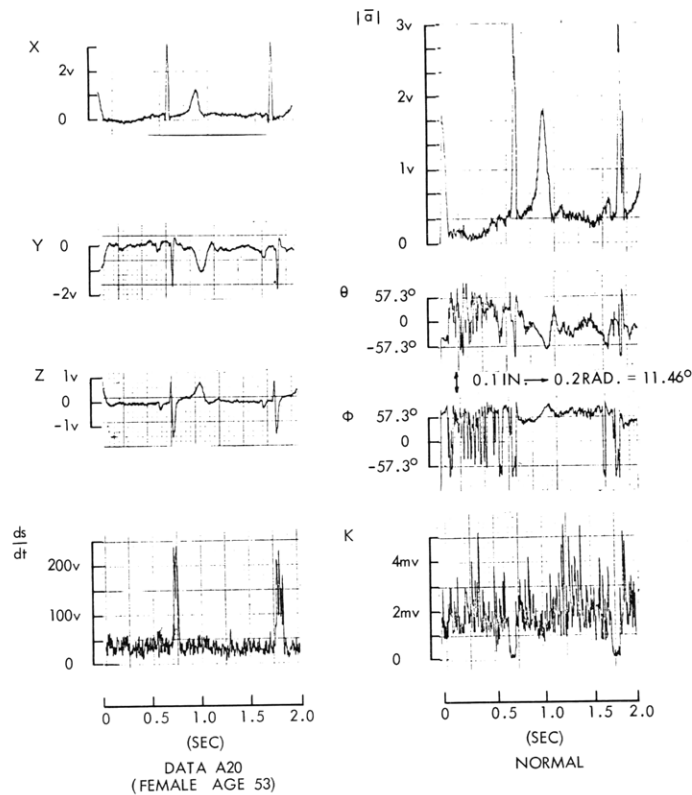


Fig. XXII-13. The EKG vector and associated functions for a normal female of age 53 years.

The spherical coordinates (spatial magnitude $|\bar{a}|$, angle of azimuth θ , and angle of elevation ϕ), the first derivative of arc speed $\frac{ds}{dt}$, and the curvature function K are all potentially valuable functions. However, further investigations of computation methods preserving signal-to-noise ratios are required. The aim is to transform the data so that we obtain three redundant vectors or alternatively that all the signal is in one vector, leaving only noise in the others. In this way the pattern-recognition program can operate only upon any one of the three redundant vectors or on the signal-bearing single vector, respectively.

We are now collecting many examples of these functions so that they may be tested by using the pattern-recognition program in order to obtain a meaningful interpretation of the data-reduction techniques.

E. Sadler, L. Stark, J. Dickson,
I. Sobel, G. Whipple

F. SOME EXPERIMENTAL PROPERTIES OF PUPILLARY NOISE

It was noticed during the investigation of pupillary noise that there is an increase in the rms noise level as the illumination level is increased. In order to investigate

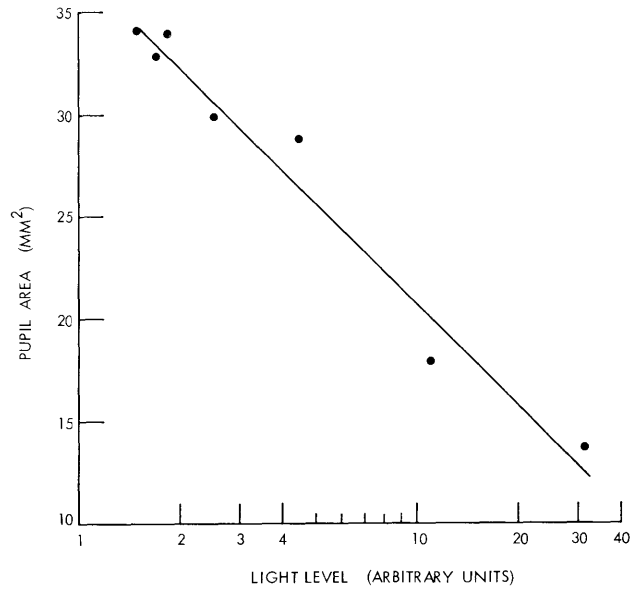


Fig. XXII-14. Pupil average area \bar{A} vs light level L .

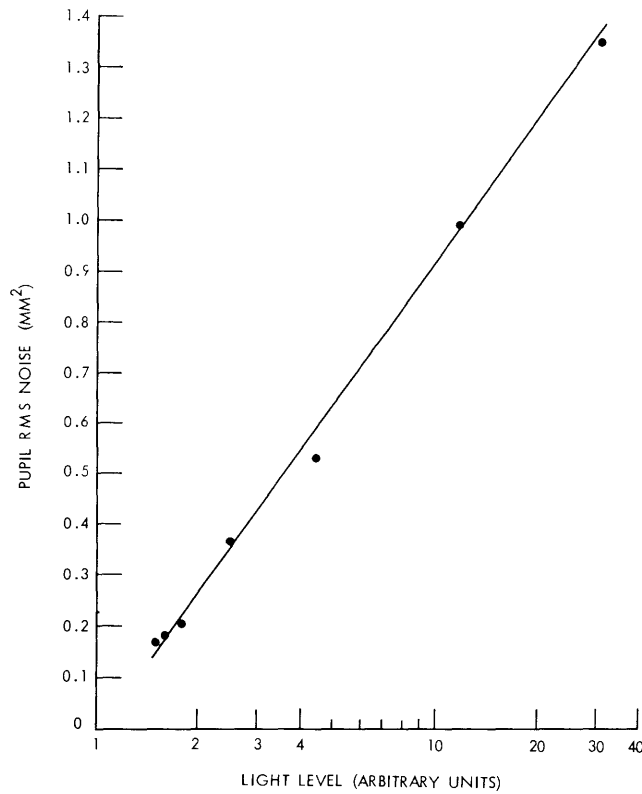


Fig. XXII-15. Pupil rms noise σ vs light level L .

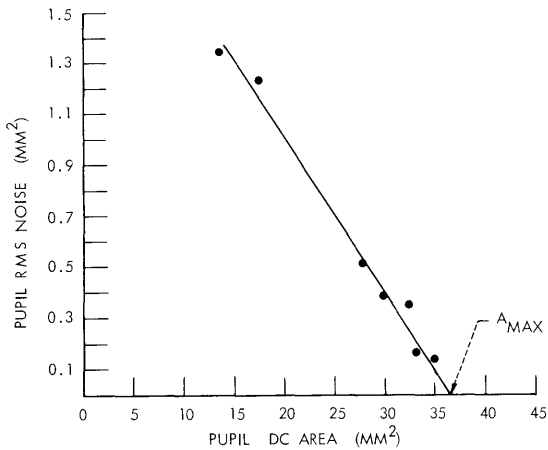


Fig. XXII-16. Pupil rms noise σ vs pupil average area \bar{A} .

this effect more fully, a program was written for the G. E. 225 computer which computed the rms and average of the pupil area signal. The experiment was performed by presenting the subject a constant light level and by measuring the rms and average area for approximately 60-80 seconds. A sampling rate of 50 samples per second was used.

Figure XXII-14 shows the average area, \bar{A} , as a function of light, L , on a semilog scale. The logarithmic dependence of \bar{A} upon L was quite expected because of various experiments on the pupil which show a logarithmic dependence of the pulse height response as a function of input pulse height. The unexpected result was the logarithmic dependence of the rms noise upon light level shown in Fig. XXII-15.

Figure XXII-16 is a graph of rms noise vs \bar{A} on a linear scale. Notice also the almost perfect linear relation between rms noise and $A_{\max} - \bar{A}$. A_{\max} is the maximum attainable average pupil area. This result might indicate that the noise is of a multiplicative nature.

In order to reinforce this hypothesis a second experiment was performed in which the pupil was stimulated by a 2-cps sinusoid and the autocorrelation of the pupil area response studied. If the hypothesis that

$$A_{\max} - A = C_1 n(t) I + C_2 I \quad (1)$$

is true, where C_1 and C_2 are constants and I is some monotonic function of L , possibly $\log L$, and if we assume that $L \approx B + D \sin \omega t$, then the autocorrelation of area signal, $R_A(\tau)$, after elimination of the constant A_{\max} term, should be

$$R_A(\tau) = \frac{C_1^2 D^2}{2} R_n(\tau) \cos \omega \tau + \frac{C_2^2 D^2}{2} \cos \omega \tau + C_1^2 B^2 R_n(\tau) + C_2^2 B^2, \quad (2)$$

where $R_n(\tau)$ is the noise source autocorrelation function.

If the additive term $(C_1^2 D^2 / 2) \cos \omega \tau$ and constant term $C_2^2 B^2$ are subtracted from $R_A(\tau)$, we should obtain

$$R_A(\tau) - \frac{C_1^2 D^2}{2} \cos \omega \tau - C_2^2 B^2 = R_n(\tau) \frac{C_2^2 D^2}{2} \cos \omega \tau + B^2 D^2 R_n(\tau). \quad (3)$$

If $R_n(\tau)$ is assumed to be approximately exponentially decreasing, then Eq. 3 is the sum

(XXII. NEUROLOGY)

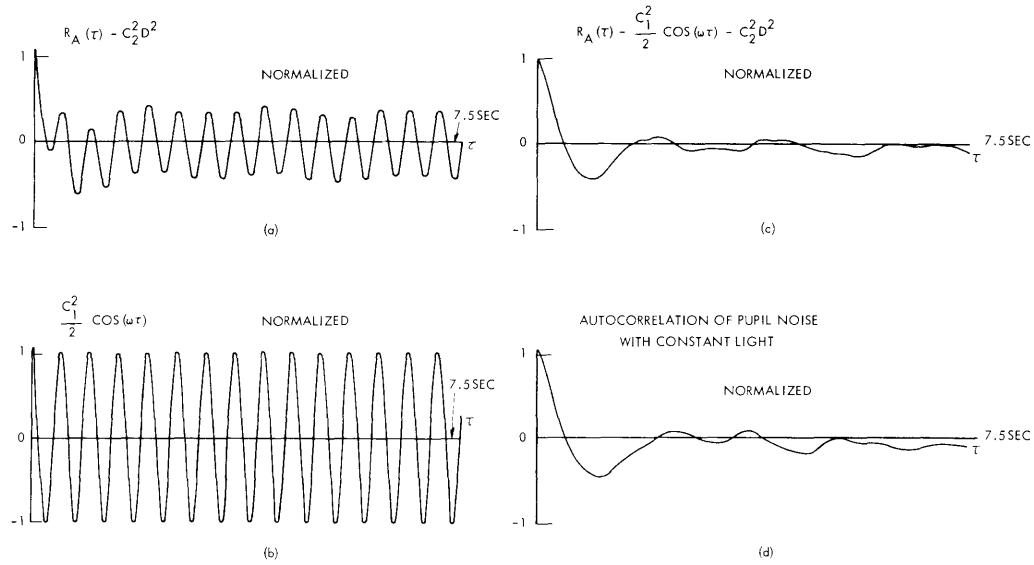


Fig. XXII-17. Autocorrelation functions of (a) pupil signal plus noise; (b) pure signal; (c) noise plus signal minus signal; and (d) noise alone.

of two terms. The first represents a signal-noise interaction term and the second, a pure noise term. The signal-noise interaction term should be an exponentially damped cosine.

A program was written for the G. E. 225 computer which accepted the autocorrelation of the pupil area, as well as the autocorrelation of the driving sinusoid, for a frequency reference, and

$$R_A(\tau) - \frac{C_1^2 D^2}{2} \cos \omega\tau - C_2^2 D^2$$

was computed. This program calculated $C_1^2/2$ by measuring the average amplitudes of oscillation of the last half section of the autocorrelation function. The experimental

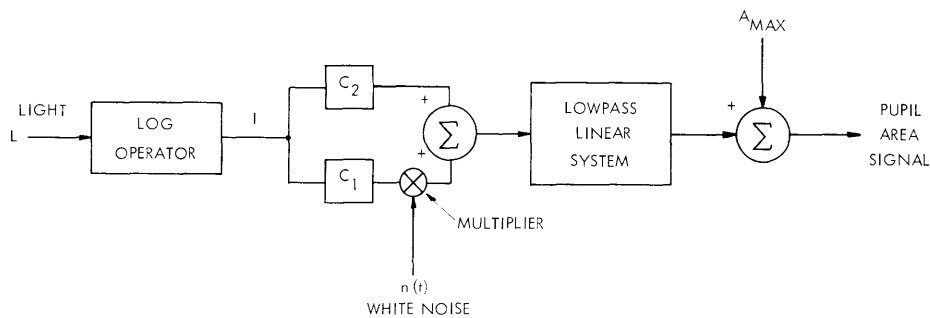


Fig. XXII-18. Simplified model to explain results of pupil noise experiments.

results are shown in Fig. XXII-17. Each autocorrelation was made up of 4 pieces of datum, each 60 seconds in length and bandpass filtered (0.03-10 cps) in order to eliminate low-frequency trends.

It is important to note that in Fig. XXII-17c we do not get a damped oscillatory behavior as might be predicted from Eq. 3. As a matter of fact, when the additive portion of the signal was subtracted, all that remained was an autocorrelation that looked like the autocorrelation of pupillary noise under constant-illumination conditions, as shown in Fig. XXII-17d for comparison purposes. This result might be described by the model shown in Fig. XXII-18 in which a lowpass filter is added after the noise is introduced into the system, in order to obtain the observed spectral characteristics.

S. F. Stanten, L. Stark

G. OPTOKINETIC NYSTAGMUS: DOUBLE STRIPE EXPERIMENT

This work is a continuation of previous studies of the optokinetic nystagmus in man.^{1,2} Earlier reports contain descriptions of both the apparatus and



Fig. XXII-19. Records of optokinetic nystagmus.

(XXII. NEUROLOGY)

the optokinetic nystagmus reflex.¹⁻⁴

In the "unfixated" case (there is no fixation point) the subject is directed only to maintain a forward gaze. His visual field is dominated by a pattern of moving, vertical stripes. With reasonably high stripe velocities ($w_f = 40-50^\circ/\text{sec}$), the nystagmus is occasionally halted, the last pursuit movement smoothly decelerating. After a period

of slow or zero velocity, the first one or two pursuit movements generally accelerate smoothly, later pursuit movements in the optokinetic nystagmus sequence having constant velocities. The deceleration, acceleration, and segments of slow or zero eye movement interrupting the optokinetic nystagmus can be seen in Fig. XXII-19a.

Figure XXII-20a shows the same data as Fig. XXII-19a. The saccadic returns have been cut away, and the smooth pursuit movements pieced together and thus the independence of pursuit and saccadic segments of optokinetic nystagmus is emphasized. The small peak on the horizontal section between the sections of optokinetic nystagmus shows that the independence is not complete. In Fig. XXII-19b and 19c two additional records of nystagmus are shown. Figure XXII-19b is the result of stripes moving from left to right, while Fig. XXII-19c results from left-moving stripes, as indicated by the different directions of the slow phases.

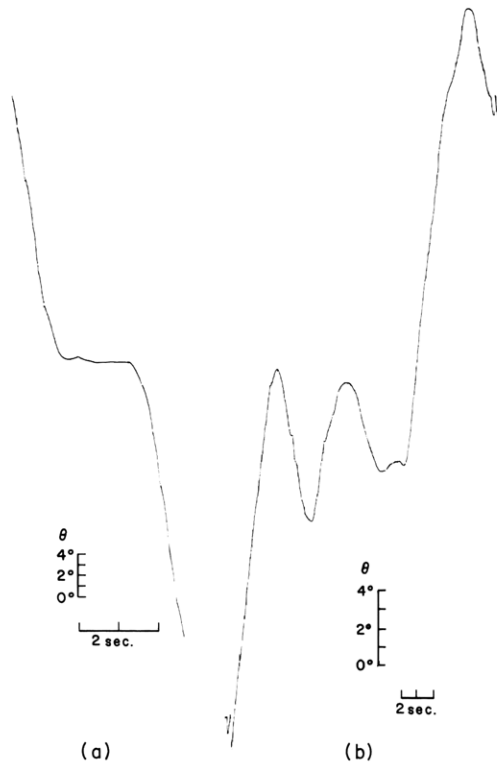


Fig. XXII-20. Constructed sequences of slow phases.

Figure XXII-19d shows eye movements resulting from the two sets of stripes presented simultaneously that generated the optokinetic nystagmus in Fig. XXII-19b and 19c. In this experiment, the stripe velocities were both approximately $9^\circ/\text{sec}$. The filtered derivative is shown at the top of Fig. XXII-19. Discrete optokinetic nystagmus segments in both directions are connected with accelerating and decelerating pursuit movements that are similar to those noted in the single-stripe experiments. Occasionally, the decelerating-accelerating movements are connected without an intervening saccade, resulting in a hump between the two directions of optokinetic nystagmus.

Figure XXII-20b shows the data in Fig. XXII-19d with the saccades taken out and the

smooth movements joined. The changes in optokinetic nystagmus that result from left-moving stripes becoming right-moving stripes can be seen as a smooth change in velocity from positive to negative.

E. G. Merrill, L. Stark

References

1. L. Stark and G. Nelson, Optokinetic nystagmus, Quarterly Progress Report No. 64, Research Laboratory of Electronics, M.I.T., January 15, 1962, pp. 326-328.
2. G. P. Nelson and L. Stark, Optokinetic nystagmus in man, Quarterly Progress Report No. 66, Research Laboratory of Electronics, M.I.T., July 15, 1962, pp. 366-369.
3. L. Stark and A. Sandberg, A simple instrument for measuring eye movements, Quarterly Progress Report No. 62, Research Laboratory of Electronics, M.I.T., July 15, 1961, pp. 268-270.
4. G. P. Nelson, L. Stark, and L. R. Young, Phototube glasses for measuring eye movements, Quarterly Progress Report No. 67, Research Laboratory of Electronics, M.I.T., October 15, 1962, pp. 214-216.

